Hybridized plasmon resonant modes in molecular metallodielectric quad-triangles nanoantenna

Arash Ahmadivand *, Raju Sinha, Nezih Pala

Department of Electrical and Computer Engineering, Florida International University, 10555W Flagler St., Miami, FL 33174, USA

ABSTRACT

In this study, we examined the plasmon response for both metallic and metallodielectric nanoantennas composed of four gold (Au) triangles in a quadrumer orientation. Tailoring an artificial metallic quad-triangles nanoantenna, it is shown that the structure is able to support pronounced plasmon and Fano resonances in the visible spectrum. Using plasmon transmutation effect, we showed that the plasmonic response of the proposed cluster can be enhanced with the placement of carbon nanoparticles in the offset gaps between the proximal triangles. It is verified that this structural modification gives rise to formation of new collective magnetic antibonding (dark) plasmon modes. Excitation of these subradiant dark modes leads to formation of narrower and deeper Fano resonances in the spectral response of the metallodielectric nanoantenna. To investigate the practical applications of the metallodielectric structure, we immersed the nano-assembly in various liquids with different refractive indices to define its sensitivity to the environmental perturbation as a plasmonic biological sensor.

© 2015 Elsevier B.V. All rights reserved.

1. Introduction

Plasmon resonances in metallic molecular clusters have been extensively utilized in designing ultra-sensitive biochemical sensors, routers, optical modulators, and long-range plasmon wave-guides [1–4]. Tailoring self-assembled nanoparticle (NP) aggregates in symmetric and antisymmetric orientations leads to support of strong subradiant dark and superradiant bright modes in nanoclusters depending on their complexity [5]. In the non-retarded limit, a weak and destructive interference between dark and bright resonant modes in the energy continuum of the dark mode gives rise to formation of pronounced Fano resonant (FR) modes in the extinction profile [6]. In terms of structural properties, spherical NPs are the most important types of metallic components that have a wide range of utilization in designing simple and complex molecular clusters, supporting plasmon resonances with tunable structural parameters [1–6]. Mie scattering and plasmon hybridization theories are the methods to analyze the plasmon response of subwavelength clusters composed of spherical particles [6,7]. However, non-spherical shapes of NPs such as nanostars, nanorices, nanospirals and bow-ties have been used extensively to design novel devices such as nanoantennas, sensors, and switches with significant sensitivity and responsivity [8,9]. For instance, just recently Nguyen et al. [10] have proved that metallic

nanostars are promising nanostructures to optimize the accuracy of detection in DNA sensing and cell reorganization due to their special geometrical flexibility for supporting plasmon resonances which makes these structures highly sensitive to the extremely subtle environmental perturbations. Nanosize spiral is another example of antisymmetric unconventional structures that was tailored to support strong FR mode in a wide range of sensing applications with significant accuracy [11]. The unique properties of non-spherical structures persuaded researchers to utilize these NPs in designing plasmonic sensors with high tunability and ultrasensitivity. As a specific case and for triangular NPs, Nein et al. [12] have proved that a metallic configuration composed of a couple of equilateral nanotriangles is able to support plasmon resonant modes in the range of visible to the near infrared region (NIR). This work also showed that strong coupling of plasmon resonant modes in a couple of metallic equivalent triangles yields resonance extremes regarding the bright and dark modes in the near-field coupling regime [10,12–14].

In this article, we examine the plasmonic response of a symmetric subwavelength nanocomplex composed of four Au triangles as a "quad-nanotriangles antenna (QNTA)" on a quartz (SiO$_2$) substrate that are placed in a head-to-head position with a certain offset distance away from each other. Using numerical analysis, we calculated the scattering cross-sectional profile for the structure under illumination with an incident linear light source. We showed that the proposed QNTA supports pronounced FR modes in the visible spectrum despite of its simple and symmetric orientation. Then, we evaluated the behavior of the FR dip with

* Corresponding author.
 E-mail address: aahma011@fiu.edu (A. Ahmadivand).

dielectric nanospheres of different dimensions (carbon (C) nanospheres (CNSs)) in the offset region between nano-triangles (metallodielectric nanoantenna). Immersing the proposed metallodielectric nanoantenna in a liquid ambience with different refractive indices and observing the behavior of FR dip during environmental perturbations we calculated the sensitivity of the nano-assembly as a biological plasmonic sensor.

2. Numerical method setup

To analyze the plasmon response of the proposed QTNA, three-dimensional (3D) finite-difference time-domain (FDTD) model (Lumerical FDTD package) was used as a numerical tool. We used the following settings for FDTD simulations: The spatial cell sizes (mesh dimensions) are set to $d_x = d_y = d_z = 1$ nm, with 12,000 number of cells, and Perfectly Matched Layers (PMLs) as the boundary condition with 64 layers. Technically, PMLs are artificial absorbing layers for scattered electromagnetic (EM) waves that are used to make the computational workplace finite. This is necessary, because any reflections will travel through the lower computational surface and cannot be separated from the forward and backward scattered EM waves. Additionally, considering numerical stability for the nanoantenna, simulation time step is set to the 0.02 fs according to the Courant stability. Courant stability is an important and necessary condition for convergence of distributed EM field during solving differential equations in numerical FDTD simulation method. It should be underlined that the applied time step must be less than a given time in explicit time integration mechanisms to yield correct outcomes.

We excited the FR modes by satisfying the condition for the interference of dark and bright modes in the metallic triangle-based nanoantenna. Fig. 1(a) shows a three-dimensional schematics of the proposed QNTA on a quartz substrate with the description of geometrical parameters inside. Each one of the equilateral triangles has identical side length of 80 nm, and the

thickness of 50 nm, where the head-to-head distance between the proximal triangles is 12 nm to provide strong coupling of plasmon resonances. This offset gap plays a key role in molecular clusters by providing a condition for interference of dipolar and multipolar modes with high energies. It has been shown that large junction distance leads to disappearance of strong plasmon resonant peaks, and in contrast, short junction distance allows strong plasmon resonances with a blue-shift to the shorter wavelengths [15,16]. Here, we set this parameter to an intermediate value to obtain strong coupling regime without blue-shift of Fano and plasmon resonant peaks. Furthermore, we used artificial apex equilateral nanotriangles for our numerical simulations in both metallic and metallodielectric QNTAs. To analyze apex nanotriangles, we used small mesh sizes for all of the axes (sub-nanoscale atomic dimensions) in the FDTD simulations. In terms of chemical compositions, Au nanotriangles and quartz substrate with the experimentally determined Johnson–Christy [17] and [18] constants were employed, respectively.

3. Results and discussion

For a regular dimer composed of two equivalent Au nanotriangles that are suited in a head-to-head position, Nein et al. [12] have analyzed the intensification of the EM field and enhancement of plasmon resonances in a metallic contour bow-tie on a dielectric substrate analytically and numerically. Using almost analogous mechanism based on plasmon hybridization concept, we induced dipolar and multipolar plasmon resonant modes in the proposed QNTA by exposing the structure to a linear plane wave, which is in the z direction with the bandwidth of $\lambda \sim 0.4$–1 µm. Fig. 1(b) exhibits the scattering cross-section diagram for a metallic triangular nanoparticles in a simple dimer orientation under transverse and longitudinal excitation. Two distinct extremes appear for electric dipolar and quadrupolar modes for both incident modes. Fig. 1(c) displays the numerically calculated scattering and
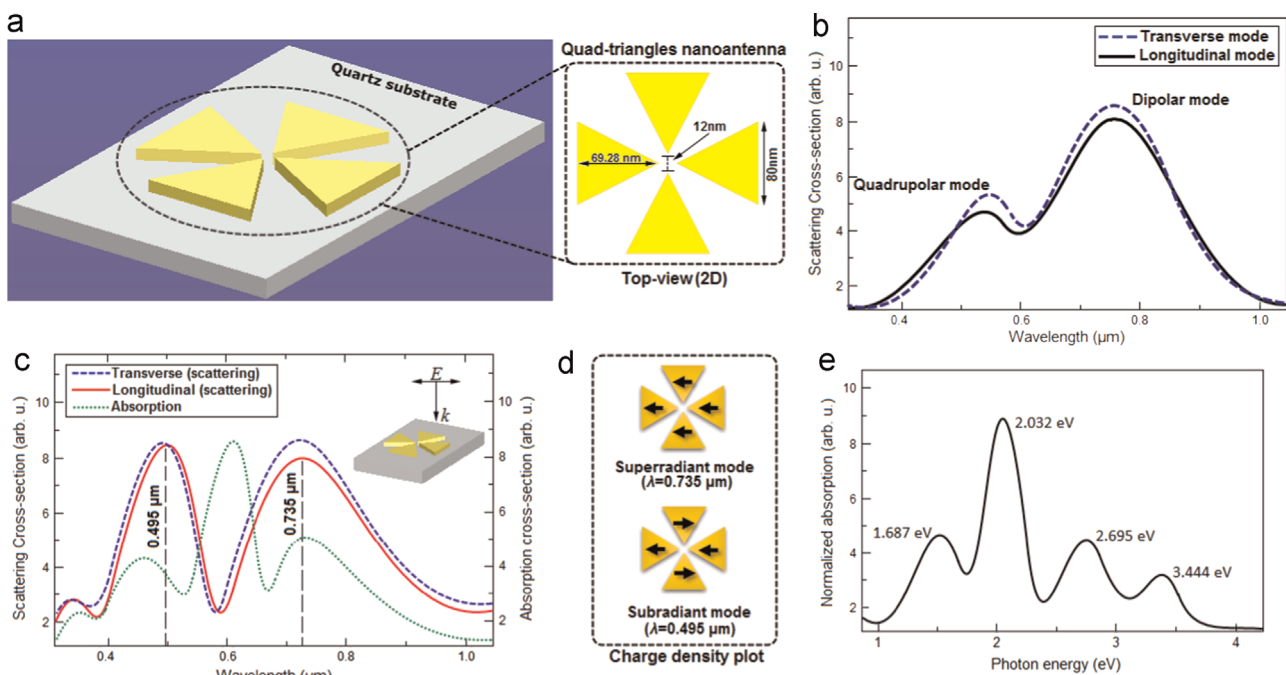
Fig. 1. a) Three and two-dimensional schematic diagrams of the QNTA on a quartz substrate with the description of geometrical parameters and sizes, b) scattering cross-sectional profile for a simple dimer of metallic triangles under transverse and longitudinal polarization excitations, c) scattering and absorption cross-sectional figures for a QNTA structure under transverse and longitudinal electric polarization modes. Inset picture shows the illumination direction and source position graphically, d) change density distribution inside the triangular quadrumer in dark and bright modes, e) normalized classical absorption diagram per photon energy ($h\upsilon$) in a QNTA.

absorption cross-section spectra for a metallic QNTA. Using Discrete Dipole Approximation (DDA) technique for non-spherical objects [19,20] and considering numerically calculated scattering diagram, two distinct plasmon resonance extremes corresponding to the superradiant bright and subradiant dark modes are identified in the visible spectrum at $\lambda \sim 0.735\ \mu m$ and $0.495\ \mu m$, respectively. Also in Fig. 1(b), a significant minimum corresponding to the FR mode is observed at $\lambda = 0.595\ \mu m$. This Fano dip is resulted from the interference between bright and dark resonant modes of the adjacent nanotriangles. Noticing in the scattering diagrams, the proposed plasmonic nanoantenna gives almost identical response to the illumination of both incident transverse and longitudinal polarizations due to its symmetric geometry with only a few nanometer shift in the position of the Fano minimum. To understand the origin of the dark and bright mode formations, it is helpful to examine the scattering cross-section profile for a dimer structure (see Fig. 1(b)). For this structure, we observed two shoulders corresponding to the dipolar and multipolar modes. In this profile, no Fano dip appears due to absence of destructive interference of dark and bright modes. To induce Fano-like or pronounced Fano dips in the scattering spectra of a metallic molecular cluster, additional structural and modal engineering is required. Symmetry breaking is one of the important mechanisms that have been utilized to create and intensify the energy of dark modes in colloidal systems [16]. The other method is the placement of nanoparticles inside the cluster to break the symmetry and generate strong dark modes such as metallodielectric structures [5]. Moreover, placement of simple nanoparticle assemblies in a close proximity to each other leads to constructive interference of the excited dipolar and multipolar modes with each other. Using this method for the data in Fig. 1(b), we analyzed creation of Fano resonant mode in the proposed triangle-based quadrumer antenna. First of all, a constructive interference between dipolar electric modes gives rise to formation of a distinct extreme regarding the superradiant bright mode. In this regime the position of superradiant bright mode peak remains fixed. On the other hand, as a result of interaction of dipolar and multipolar resonant modes, a distinct dark mode can be obtained in the scattering spectra with a dramatic blue-shift in the position of the peak. The result of interaction between the dark and bright modes is formation of a noticeable dip between them in the visible frequency. In addition, the direction of charge density for both dark and bright modes is plotted in Fig. 1(d). Considering the absorption curve in Fig. 1(c), the peak of the plasmon resonance absorption appears at the wavelength of FR dip, and also, two other absorption shoulders are observed at the wavelengths of dark and the bright resonant modes, which is in complete agreement with the hybridization theory. The inset shows the propagation direction

and polarization of the incident wave graphically. To understand the plasmonic response by the plasmon hybridization theory and to obtain the energy level diagram, we plotted the classical normalized absorption diagram over the incoming photon energy ($h\upsilon$) (see Fig. 1(e)). This profile also helps to understand the amount of accumulated plasmon resonance energy and intensity of localized and hybridized plasmon modes on the spot at the middle of the QNTA. Noticing in the normalized absorption profile, four distinct shoulders correlating with the localized surface plasmon resonances (LSPRs) are observed at 1.687/2.032/2.695/3.444 eV. The distinct peak at 2.032 eV is related to the FR mode position in the coupling spot at the center of the metallic QNTs. Fig. 2 shows the simulated two-dimensional E-field distribution for the plasmon resonance excitation and localization at the center point between the Au nanotriangles for the frequencies of dark, bright, and FR modes under transverse polarization excitation. Applying plasmon hybridization theory to analyze the behavior of FR dip, we observed strong localization and accumulation of plasmon resonant modes at the center point between the Au nanotriangles (in the offset gap position between head-to-head particles), which leads to generation of hot spots and large amount of energy dissipation.

We plotted the energy level diagram for the QNTA based on triangle NP dimer (NPD) and triangle cavity dimer (NCD) in Fig. 3. The energy level diagram is plotted for three different states of a triangle-based nanostructure unit which are QNT, NPD, and NCD separately. To this end, we illuminated the cavity and particle dimers individually to determine the amount of photon energy absorption for the corresponding resonant modes which are denoted by $|\omega_\pm>_{NPD}$ and $|\omega^\pm>_{NCD}$ for the bonding bright and the antibonding dark modes. Besides, four energy peaks are identified at different levels, wherein the mode that appears at 1.687 eV corresponds to $|\omega^->_{QNT}$, which is formed by the plasmon bonding modes of NPD and NCD systems ($|\omega_->_{NPD} \leftrightarrow |\omega^->_{NCD}$). The second energy level is 2.032 eV corresponding to $|\omega^+>_{QNT}$, which is formed by the interference of bonding and antibonding modes of the cavity and the NP dimers energies with the contribution of bonding mode ($|\omega_->_{NPD}$) as: (($|\omega_->_{NPD} + |\omega_->_{NPD}$) $\leftrightarrow |\omega^->_{NCD}$). The other resonant mode with the energy level at 2.695 eV is the third plasmon resonant mode ($|\omega_+^->_{QNT}$) that is formed by the interaction of a mixture of bonding and antibonding modes of the dimer NPs and a bonding mode of cavity dimer as: ($|\omega_->_{NPD} + |\omega_+>_{NPD}$) $\leftrightarrow |\omega^+>_{NCD}$. The last mode is the resonant mode that is observed at the energy of 3.444 eV ($|\omega_+^+>_{QNT}$) and resulted by the interference of antibonding plasmon modes as: $|\omega_+>_{NPD} \leftrightarrow |\omega^+>_{NCD}$. So far, we examined the plasmon responses for a symmetric metallic QNTA which includes a pronounced FR minimum in the visible spectrum. To understand the operation mechanism of the presented nanoantenna, we plotted the charge density distribution inside the
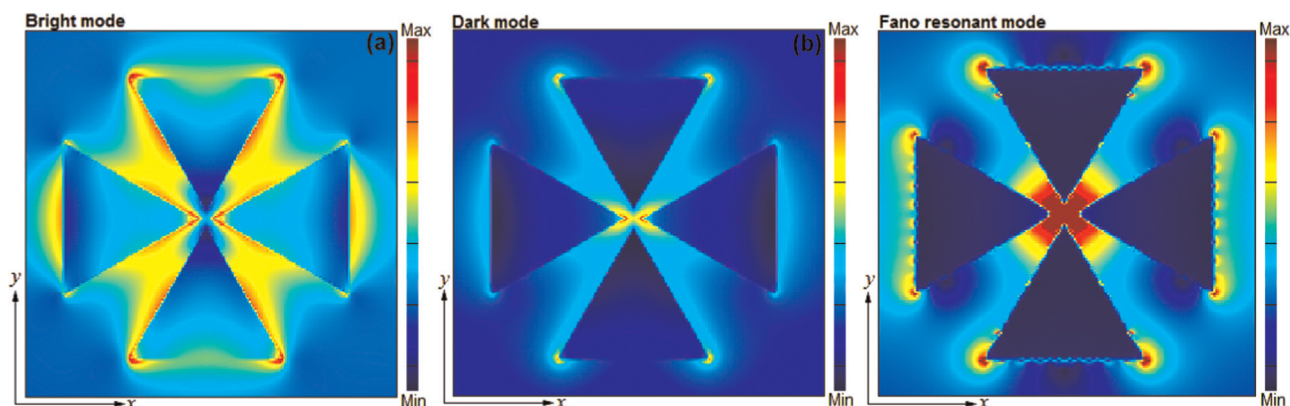
Fig. 2. a, b, c) Two-dimensional simulation snapshots of plasmon resonance excitation and coupling for the bright ($\lambda \sim 0.495\ \mu m$), dark ($\lambda \sim 0.630\ \mu m$), and FR modes ($\lambda \sim 0.595\ \mu m$), respectively.
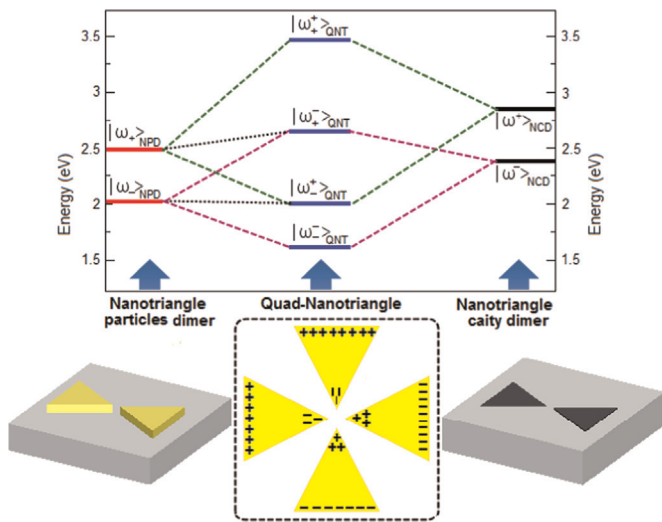
Fig. 3. Energy level diagram for the plasmon resonance hybridization in a QNTA configuration with the charge distribution diagram.

triangles in the metallic QNTA structure for FR position ($\lambda = 0.595$ μm) in Fig. 3.

Next, we investigate the spectral response for the same nanoantenna with the addition of CNSs in the junction space between proximal Au triangles as metallodielectric structures. Noticing in Fig. 4(a), four amorphous CNSs are deposited in the top sections between nanotriangles with variable radii. Wen et al. [21]

and Ahmadivand et al. [22] have verified that addition of dielectric NPs in a metallic molecular assembly of spherical particles gives rise to formation of new collective magnetic subradiant (dark) magnetic modes, which provide a significant contribution to the excitation of strong and deep FR dips. Fig. 4(b) shows the plasmon response of a metallodielectric QNTA with the presence of CNSs of three different sizes. Here, using identical CNSs with the diameters in the range of 6/7/8 nm, a pronounced Fano minimum is induced in the scattering profile, and a significant enhancement in the FR dip is obtained by increasing the size of CNSs. Technically, increase of the size of the CNSs, causes the increase in the energy of the collective dark modes and improvements in the quality of FR with red-shift to the longer wavelengths. This pronounced Fano minimum appears at $\lambda = 0.695$ μm that is resulted from the contribution of collective magnetic dark modes in the presence of CNSs with the diameter of 8 nm. It should be underlined that new strong dark resonant modes induce quadrupolar magnetic plasmon resonances in the pronounced FR mode and improve its performance. Fig. 4(c) illustrates the simulated two-dimensional E-field distribution for the case of plasmon hybridization and localization enhancements in the studied nanoantenna with the presence of CNSs. The strongest field intensities are identified in the offset gap distance (the position of CNSs) between triangles.

Finally, we used the metallodielectric QNTA to design a nanoscale plasmonic sensor. To this end, four different chemical fluids with different refractive indices were used to examine the sensitivity of the presented metallodielectric QNTA. Fig. 5 (a) shows a schematic diagram of the proposed plasmonic structure that is immersed in a liquid system completely. Calculating
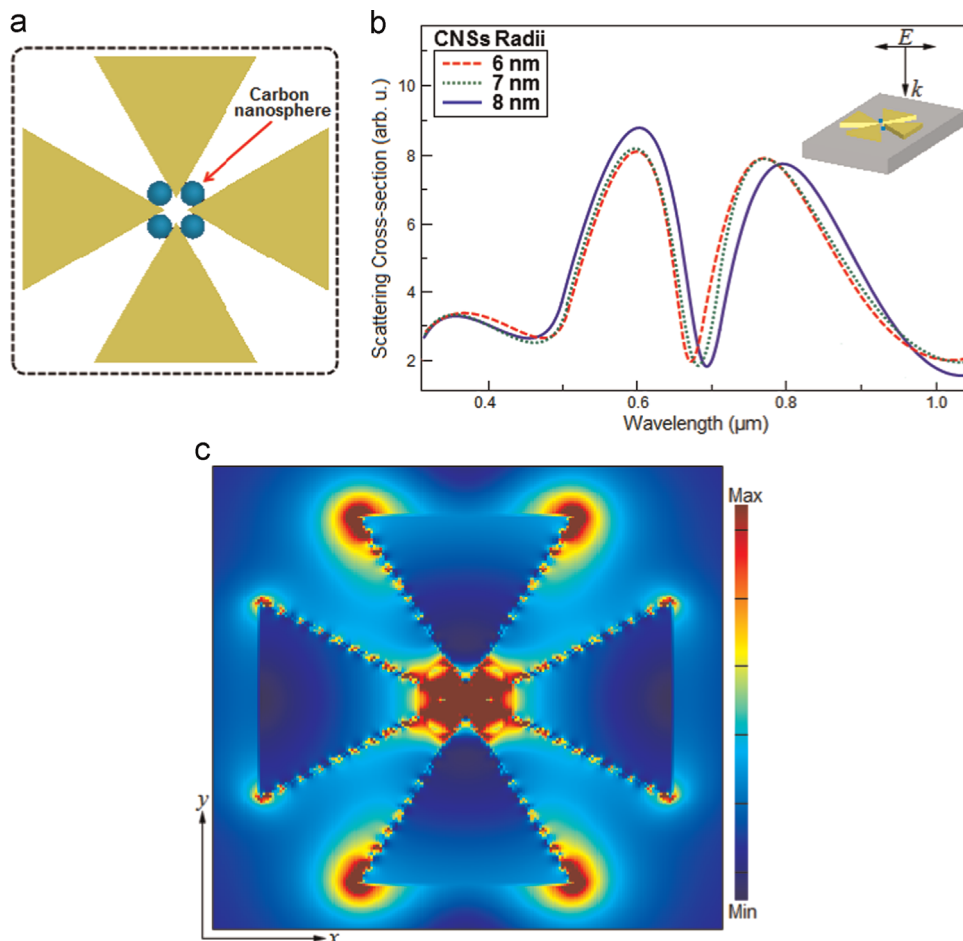
Fig. 4. a) A two-dimensional schematic diagram of the QNTA with the placement of CNSs, b) scattering cross-sectional profile for the QNTA with the presence of CNSs, c) two-dimensional simulation snapshot for a QNTA composed of CNSs for the FR mode ($\lambda \sim 0.695$ μm).
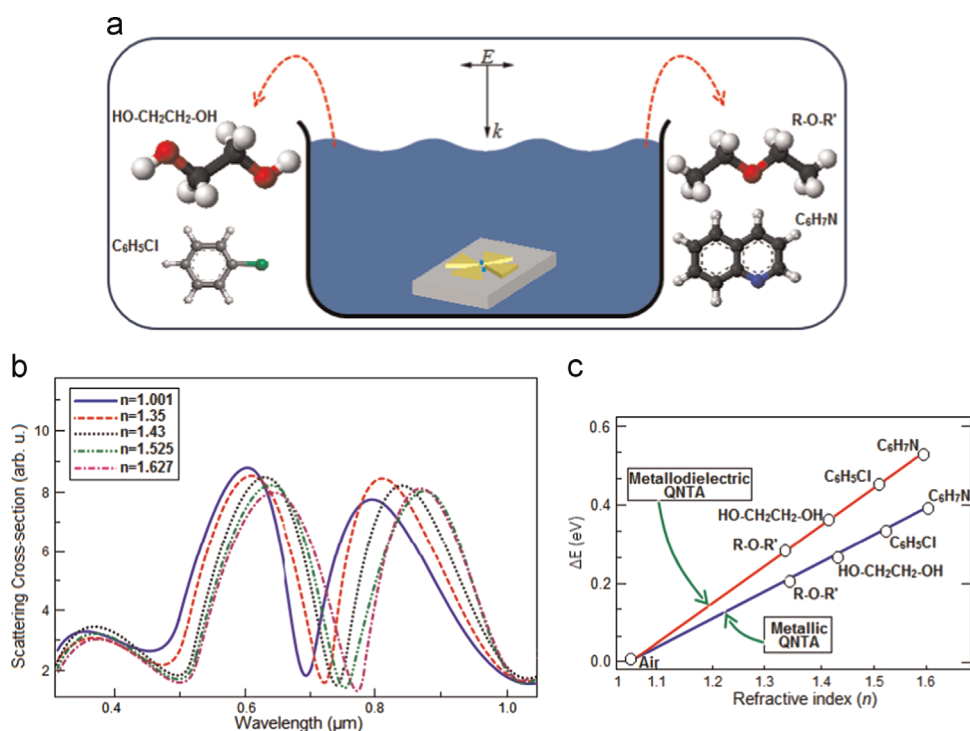
Fig. 5. a) A schematic diagram of a nanoantenna in a fluid system with the chemical formulations of immersed liquids, b) scattering cross-sectional profile for the QNTA with CNSs in a medium with the variable refractive index, c) a linear plot of plasmon resonance energy deviations over the refractive index variations as a FOM profile.

the scattering spectra for the structure, we examined the response of the metallodielectric QNTA to the environmental refractive index perturbations. The sensitivity of the structure is quantified by the widely used figure of merit (FOM). The FOM is defined by the ratio of the plasmon resonance energy shifts (ΔE) over the refractive index (n) variations as a linear fit. We used following fluids as a surrounding ambience: Ether (R–O–R') with $n=1.35$, Ethylene glycol (HO–CH_2CH_2–OH) with $n=1.43$, Chlorobenzene (C_6H_5Cl) with $n=1.525$, and Quinoline (C_6H_7N) with $n=1.627$ [23–25]. Fig. 5(b) showsa comparative diagram for the spectral response of the QNTA to the refractive index variations, where a noticeable red-shift in the position of FR minima to the longer wavelengths is observed with the increasing refractive index of the medium. Considering the previously proposed methods to determine the FOM value for the designs with an antisymmetric FR dip [15,16], we calculated it for the studied metallodielectric QNTA as ~8.25 (see Fig. 5(c)). The obtained value of FOM is a significant value for a simple molecular and symmetric structure, comparing to the one for a fully metallic QNTA (~7.7), showing the superior performance of the metallodielectric QNTA (see Fig. 5(c)). It should be noted that increasing the number of QNTA and depositing them on a metasurface as meta-atoms could provide a pathway to design a plasmonic metamaterial that is a potential candidate with an outstanding FOM for biochemical sensing applications.

4. Conclusions

We studied the plasmonic response of a nanoscale antenna composed of closely packed Au triangle NPs and the same with carbon nanospheres. We showed that presented nanostructures can be tailored to support pronounced FR modes in the visible range of spectrum. It is verified that deposition of CNSs in the certain offset gap distances between triangles gives rise to significant enhancements in the intensity of plasmon resonances and high quality FR dips. Using the proposed metallodielectric QNTA as

a plasmonic sensor, we calculated the sensitivity of the structure to the environmental refractive index perturbations. This understanding can help designing simple molecular structures that are able to support strong plasmon and Fano resonances for various sensing applications.

References

[1] Y. Zhan, D.Y. Lei, X. Li, S.A. Maier, Plasmonic Fano resonances in nanohole quadrumers for ultra-sensitive refractive index sensing, Nanoscale 6 (2014) 4705–4715.
[2] B. Yan, S.V. Boriskina, B.M. Reinhard, Design and implementation of noble metal nanoparticle cluster arrays for plasmon enhanced biosensing, J. Phys. Chem. C 115 (2011) 24437–24453.
[3] A. Ahmadivand, Hybrid photonic-plasmonic polarization beam splitter (HPPPBS) based on metal-silica-silicon interactions, Opt. Laser Technol. 54 (2014) 145–150.
[4] M. Liu, S. Mukherjee, K. Bao, Y. Li, L.V. Brown, P. Nordlander, N.H. Halas, Manipulating magnetic plasmon propagation in metallic nanocluster networks, ACS Nano 6 (2012) 5482–5488.
[5] J.A. Fan, C. Wu, K. Bao, R. Bardhan, N.J. Halas, V.N. Manoharan, P. Nordlander, G. Shvets, F. Capasso, Self-assembled plasmonic nanoparticle clusters, Science 328 (2010) 1135–1138.
[6] B. Luk'yanchuk, N.I. Zheludev, S.A. Maier, N.J. Halas, P. Nordlander, H. Giessen, C.T. Chong, The Fano resonance in plasmonic nanostructures and metamaterials, Nat. Mater. 9 (2010) 707–715.
[7] R.G. Newton, Scattering Theory of Waves and Particles, 2nd ed., Dover Publications, New York, 1982.

[8] H. Wei, A. Reyes-Coronado, P. Nordlander, J. Aizpurua, H. Xu, Multipolar plasmon resonances in individual Ag nanorices, ACS Nano 4 (2010) 2649–2654.

[9] A. Gopalakrishnan, M. Chirumamilla, F. De Angelis, A. Toma, R.P. Zaccaria, R. Krahne, Bimetallic 3D nanostars dimers in ring cavities: recyclable and robust surface-enhanced Raman scattering substrates for signal detection from few molecules, ACS Nano 8 (2014) 7986–7994.

[10] A.H. Nguyen, X. Ma, S.J. Sim, Gold nanostars based biosensor detects epigenetic alterations on promoter of real cells, Biosens. Bioelectron. 66 (2015) 497–503.

[11] S. Golmohammadi, A. Ahmadivand, Fano resonances in compositional clusters of Aluminum nanodisks at the UV spectrum, a route to design efficient and precise biochemical sensors, Plasmonics 9 (2014) 1447–1456.

[12] L.W. Nein, S.C. Lin, B.K. Chao, M.J. Chen, J.H. Li, C.H. Hsueh, Giant electric field enhancement and localized surface plasmon resonance by optimizing contour bowtie nanoantennas, J. Phys. Chem. C 117 (2013) 25004–25011.

[13] L. Li, S.F. Lim, A.A. Puretzky, R. Riehn, H.D. Hallen, Near-field enhanced ultra-violet resonance Raman spectroscopy using aluminum bow-tie nano-antenna, Appl. Phys. Lett. 101 (2012) 113116.

[14] P. Melchior, D. Bayer, C. Schneider, A. Fischer, M. Rohmer, W. Pfeiffer, M. Aeschlimann, Optical near-field interference in the excitation of a bowtie nanoantenna, Phys. Rev. B 83 (2011) 235407.

[15] A. Ahmadivand, S. Golmohammadi, M. Karabiyik, N. Pala, Fano resonances in complex plasmonic necklaces composed of gold nanodisks clusters for enhances LSPR sensing, IEEE Sens. J. 35 (2015) 1588–1594.

[16] J.B. Lassiter, H. Sobhani, J.A. Fan, J. Kundu, F. Capasso, P. Nordlander, N.J. Halas, Fano resonances in plasmonic nanoclusters: geometrical and chemical tun-ability, Nano Lett. 10 (2010) 3184–3189.

[17] P.B. Johnson, R.W. Christy, Optical constants of the noble metals, Phys. Rev. B 6 (1972) 4370.

[18] E.D. Palik, Handbook of Optical Constants of Solids, Academic Press, San Diego, USA, 1991.

[19] B.T. Draine, P.J. Flatau, Discrete dipole approximation for scattering calcula-tions, J. Opt. Soc. A 11 (1994) 1491–1499.

[20] P.K. Jain, S. Eustis, M.A. El-Sayed, Plasmon coupling in nanorod assemblies: Optical absorption, discrete dipole approximation simulation, and extinction coupling model, J. Phys. Chem. B 110 (2006) 18243–18253.

[21] F. Wen, J. Ye, N. Liu, P. Van Dorpe, P. Nordlander, N.J. Halas, Plasmon trans-mutation: inducing new modes in nanoclusters by adding dielectric nano-particles, Nano Lett., b (2012) 5020–5026.

[22] A. Ahmadivand, M. Karabiyik, N. Pala, Intensifying magnetic dark modes in the antisymmetric plasmonic quadrumer composed of Al/Al_2O_3 nanodisks with the placement of silicon nanospheres, Opt. Commun. 338 (2015) 215–225.

[23] R.C. Weast, D.R. Lide, M.J. Astle, CRC Handbook of Chemistry and Physics, CRC Press, Taylor & Francis Group, USA, 1989.

[24] H.C. Brown, E.A. Baude, F.C. Nachod, Determination of Organic Structures by Physical Methods, Academic Press, New York, 2013.

[25] J.J. McKetta, Chemical Processing Handbook, Marcel Dekker, New York, 1993.